ACS APPLIED MATERIALS & INTERFACES

Research Article

Cite This: ACS Appl. Mater. Interfaces 2019, 11, 16914−16921

www.acsami.org

Coexistence of Antiadhesion Performance, Intrinsic Stretchability, and Transparency

Minhuan Liu,[†] Fanghui Liu,[‡] Xiubin Xu,[†] Danfeng Yu,[†] Ian Wyman,[§] Hui Yang,[‡] Jinben Wang,[‡] and Xu Wu*[,†]

[†]Department of Chemistry and Chemical Engineering, Guangzhou University, Guangzhou 510006, China

[‡]Beijing National Laboratory for Molecular Sciences, Key Laboratory of Colloid, Interface and Chemical Thermodynamics, Institute of Chemistry, Chinese Academy of Sciences, Beijing 100190, China

[§]Department of Chemistry, Queen's University, Kingston K7L 3N6, Canada

Supporting Information

ABSTRACT: Antiadhesion performance, stretchability, and transparency are highly desirable properties for materials and devices in numerous applications. However, the existing strategies for imparting materials with antiadhesion performance generally induce rigidity and opacity, and principle is yet to be provided for designing materials that combine these important parameters. Here, we show that four factors including a low surface energy, appropriate cross-linking, availability of a homogeneous and amorphous composite, and a smooth material surface can be used to design an intrinsically stretchable and transparent polymer film with antiadhesion performance against various liquids including water, diiodomethane, hexadecane, cooking oil, and pump oil. The film can be obtained via simply molding a waterborne polymer network at ambient temperature. Furthermore, the film can retain its antiadhesion performance and outstanding transparency even when it is subjected to large mechanical deformations reaching up to 1800%, and its maximal fracture strain exceeds 3000%. These design concepts offer a general platform for achieving multiple material functionalities, and may open new avenues for the surface functionalization of stretchable materials and devices.

KEYWORDS: *antiadhesion performance, intrinsic stretchability, transparency, polymer film, combined parameters*

1. INTRODUCTION

The rapid advancements seen in the fields of information technology and biotechnology have allowed us to envision the future, one in which synthetic materials and devices such as artificial skin,[1,2] bionic muscles,[3,4] and wearable electronics[5,6] are widely used for prosthetics and advanced robotics. As researchers endeavor to achieve these applications to help us cure diseases and obtain capabilities once thought to be impossible, stretchability and optical transparency of materials and devices have become increasingly sought after.[1−9] On the other hand, controlling the surface wettability of materials is a classical and key issue, and antiadhesion surfaces with poor affinity to both water and oil have been designed and prepared extensively in the literature reports.[10−12] However, the existing materials with antiadhesion performance generally have structural requirements that restrict their stretchability and transparency. There is still a fundamental lack of a designing concept considering the coexistence of these highly desirable properties to achieve the surface functionalization required for the next generation of stretchable materials and devices.

In general, the materials with adhesion resistance to both water- and solvent-based liquids can be classified into three categories according to their architectures, known as hemi-air, hemi-liquid, and homogeneous solid materials, respectively. The lotus-inspired hemi-air surfaces trap air pockets in micro- and nanoscale textured materials with low surface energies, thus exhibiting superamphiphobic properties with high contact angles (exceeding 150°) and low sliding angles (below 10°) toward both water and oil.[13−15] The hemi-liquid materials with slippery liquid-infused porous surfaces (SLIPS) are inspired by the *Nepenthes* pitcher plants, containing low-surface-energy fluids that are locked in place within modified porous materials[16,17] or polymer matrixes,[18] and they yield moderate contact angles below 120° while remaining clean after exposure to various liquids. Meanwhile, as the oldest fluorinated polymer with a low surface energy as well as a homogeneous solid fluorocarbon-based structure, poly(tetrafluoroethylene) (PTFE, Teflon) can also repel a wide range of liquids at moderate contact angles, and has been successfully employed

Received: January 30, 2019
Accepted: April 16, 2019
Published: April 16, 2019

DOI: 10.1021/acsami.9b01971
ACS Appl. Mater. Interfaces 2019, 11, 16914−16921

in many demanding applications where antiadhesion performance is required.[19−21]

Unfortunately, the inherent structures of superamphiphobic, SLIPS, and PTFE-based materials inhibit their stretchability, thus restricting their applications in wearable, implanted, or epidermal materials and devices. To the best of our knowledge, no intrinsically stretchable superamphiphobic materials have been reported, as the hierarchical textured structures that hold air pockets in place are often intricate and prone to damage via mechanical deformation. By regulating the roughness of the surfaces that are damaged by deformation, a limited variety of elongated surfaces that can only repel water have been achieved. These materials were prepared by spraying hydrophobic nanoparticles onto stretchable substrates such as rubber[22] and resin,[23] or by creating micro/nanotextured roughness on monoliths with a maximum strain of ∼100%.[24] In the case of a SLIPS material, the slight stretching by less than 10% would severely degrade its liquid repellency and transparency due to the disruption of the lubricant surface layer by newly formed gaps resulting from this deformation.[25] Monolayers[26,27] or polymer-based coatings[28−31] bearing lubricant surfaces formed by the low-surface-energy fluids can provide similar antiadhesion performance as obtained with SLIPS materials. These surfaces can also exhibit transparency, although there has been a lack of studies regarding their stretchability. Lastly, it is difficult to impart PTFE-based materials with stretchability because of their poor solubility in most solvents and high melting points (∼330 °C), whereas their high melting viscosities further impede the molding of these materials into films.[32−34] In addition to their rigidity and lengthy preparation, superamphiphobic, SLIPS, and PTFE-based materials tend to scatter light due to their micro/nanoscaled roughness,[22−24] pores,[25] and crystallinity,[32−34] which can affect their transparency and render them unsuitable for applications as wearable electronics, such as displays, sensors, and actuators.[35−37]

Herein, we were able to develop a transparent polymer film that exhibits both antiadhesion performance against various liquids and high intrinsic stretchability. As will be described below and referred to later in this report, four essential structural elements were incorporated into the design of this material with a combination of desirable properties. These features included (1) a low-surface-energy component necessary for antiadhesion performance, (2) an appropriate (including both chemical and physical) cross-linking of polymers to also provide the antiadhesion performance and stretchability, (3) a homogeneous and amorphous nature to offer transparency, and (4) a smooth material surface that reliably retained its curvature during stretching, so that it was immune to deformation-induced changes of roughness and wettability that typically plague textured surfaces.

2. EXPERIMENTAL SECTION

2.1. Materials. Isophorone diisocyanate (IPDI, >99.0%), poly(tetramethylene glycol) (PTMG, with an average equivalent weight of 1000 g/mol), and dimethylolbutanoic acid (DMBA) were supplied by Hengtai Chemical Co., Ltd. Trimethylolpropane (TMP), triethylamine (TEA, ≥99%), ethanediol (ED), and ethylene diamine (EDA, ≥99%) were provided by Damao Chemical Reagent Co., Ltd. IPDI, dibutyltin dilaurate (DBTDL, Aladdin, 95%), EDA, and TEA were used as received. PTMG, TMP, EG, and DMBA were purified under vacuum prior to use. 1*H*,1*H*,2*H*,2*H*-Tridecafluoro-1-octanol (TFO) was purchased from XEOGIA and distilled under vacuum prior to use. Acetone was used after it had been dehydrated for 48 h with 4.0 Å molecular sieves.

2.2. Synthesis of FSCPN, FPN-P, and FPN-C. In a typical synthesis procedure for the fluorine-terminated synergistic cross-linked polyurethane network (denoted as FSCPN), calculated amounts of PTMG (15.0 g, 15.0 mmol), DMBA (1.48 g, 10.0 mmol), and TMP (0.67 g, 5.00 mmol) were charged into a 250 mL flask, and the mixture was purged with nitrogen for 30 min at room temperature. IPDI (11.1 g, 50.0 mmol), DBTDL (0.0100 g, 0.0160 mmol), and acetone (5.00 mL) were added to the flask, and the reaction proceeded for 2 h at 80 °C. TFO (3.64 g, 10.0 mmol) was subsequently added into the above mixture, and the reaction was allowed to continue for 2 h. This reaction mixture was cooled to 40 °C, and TEA (1.01 g, 10.0 mmol) was used to neutralize the DMBA units. Finally, an aqueous solution (78.6 g) comprising EDA (0.75 g, 12.5 mmol) was added dropwise under vigorous stirring to obtain a 30.00 wt % FSCPN aqueous solution. The fluorine-terminated polyurethane networks with either physical or chemical cross-linking (denoted as FPN-P and FPN-C, respectively) were prepared via similar procedures, except that ED (0.47 g, 7.50 mmol) was used instead of TMP for the preparation of FPN-P, and ED (0.78 g, 12.5 mmol) was added and allowed to react for 2 h prior to the cooling of the reaction mixture, although the addition of EDA was not performed during the preparation of FPN-C.

2.3. Preparation of the Films. The FSCPN/FPN-P/FPN-C aqueous solutions were poured into a culture dish at 50 °C for 24 h to form the films. The films were then peeled from the culture dish and cut into rectangle pieces for further testing.

2.4. Characterization Methods. The energy-dispersive X-ray spectroscopy (EDX) elemental mapping of the films was conducted using a scanning electron microscope (SEM, Hitachi, SU8010), which was operated at an accelerating voltage of 20 kV. The elemental analysis of both sides of the film was performed by X-ray photoelectron spectroscopy (XPS, Thermo Scientific, ESCALAB 250Xi). Size-exclusion chromatography (SEC) analysis was performed using a Waters 515 system equipped with a guard column. The molecular weight of FSCPN was determined using polystyrene standards, and tetrahydrofuran was used as the mobile phase at a flow rate of 1.0 mL/min. The aggregates that formed in aqueous FSCPN solutions were observed with a transmission electron microscope (TEM, JEOL, JEM-2100F). The solution was added dropwise onto a 400-mesh carbon-coated copper grid, frozen using liquid nitrogen, and then dried under vacuum to prepare the TEM samples. Fourier-transform infrared (FTIR, Bruker Optics, Spectrum 100) spectra recorded with a Tensor-27 spectrometer were employed to monitor the consumption of the isocyanate groups, and KBr was used as the sample matrix. The contact angle (CA), sliding angle (SA), advancing contact angle (θ_A), and receding contact angle (θ_R) were measured using a contact angle measuring instrument (Shengding, JC2000A). The θ_A and θ_R were, respectively, measured by injecting the test liquids into or withdrawing them from a droplet resting on the film until it advanced or receded. Each reported contact angle or sliding angle corresponded to the average of five measurements. Thermal stability measurements were conducted via thermogravimetric analysis (TGA, Perkin Elmer, TGA4000) using dry nitrogen as the purge gas. Differential scanning calorimetry (DSC, Perkin Elmer, DSC8000) was performed under a nitrogen atmosphere with the heating and cooling rates of 10 °C/min. Mechanical tensile-stress tests were performed using a universal testing machine (SUNS, UT4304) with a load cell of 100 kN. The microphotographs were recorded using an optical microscope (Mshot, MD30). The recovery ratio was calculated by the equation: $R_r = 1 - \varepsilon_{(t)}/\varepsilon_{max}$, where ε_{max} is the strain measured at the beginning of the recovery process and $\varepsilon_{(t)}$ is the time-dependent strain. An atomic force microscope (AFM, Bruker, Dimension) was used to analyze the surface roughness of the film. Dynamic thermomechanical analysis (DMA) was conducted using a dynamic mechanical analyzer (TA instrument, Q800). Meanwhile, the optical transmittance of the film was measured using a UV−vis spectrophotometer (Perkin Elmer, Lambda 950).

DOI: 10.1021/acsami.9b01971
ACS Appl. Mater. Interfaces 2019, 11, 16914−16921

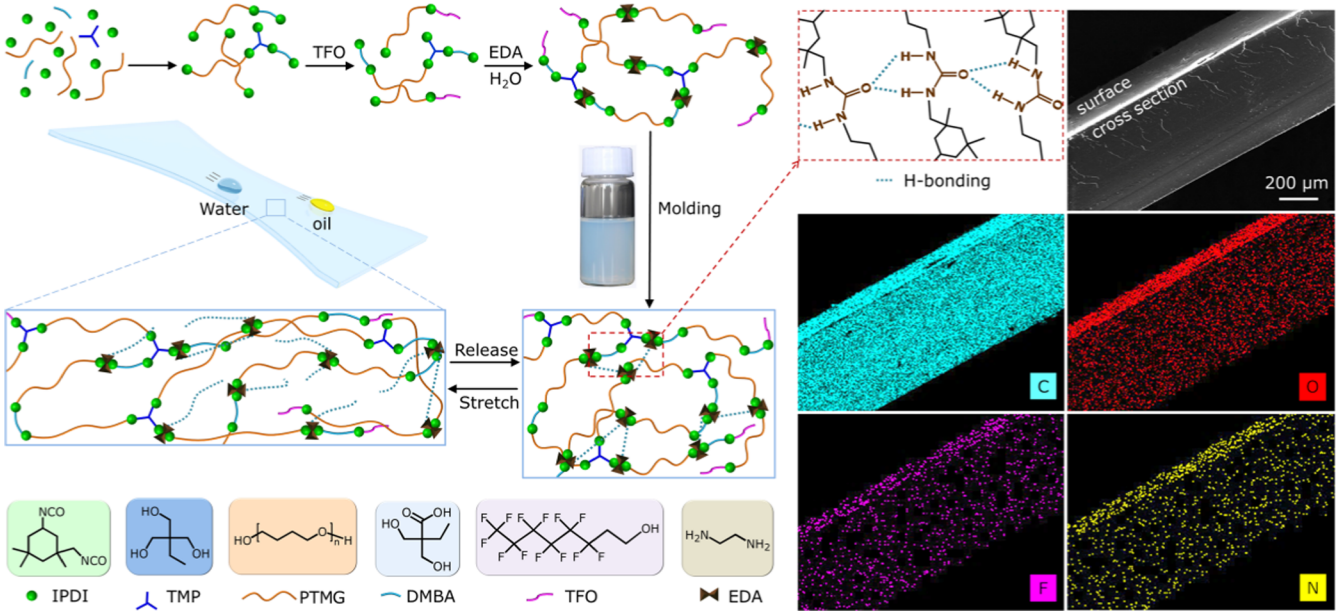

Figure 1. Design and synthesis of the FSCPN film, as well as the SEM and EDX mapping of the film's cross section.

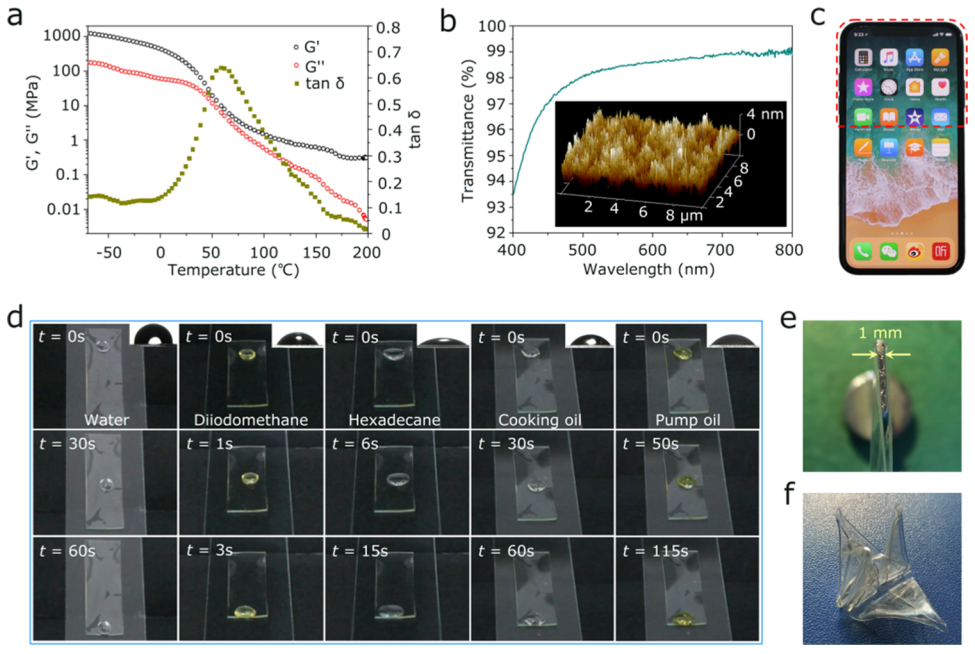

Figure 2. Transparency, antiadhesion performance, and flexibility of the films. (a) G', G'', and tan δ (G''/G') curves of the film obtained via DMA. (b) Optical transmission measurements of the film, including an inset AFM image of the film surface. (c) Photograph of a smartphone screen covered by the film in the top region that is outlined by red dashed lines. The remaining region at the lower sections of the screen was left uncoated for comparison. (d) Photographs of various liquids sliding off the film. (e) Photograph taken during the measurement of the film's minimum bending radius. (f) Photograph of a film sample that had been folded into a crane shape.

3. RESULTS AND DISCUSSION

The film developed in this work was simply molded in a culture dish at 50 °C for 24 h from a fluorine-terminated synergistic cross-linked polyurethane network (FSCPN, Figure 1) that was dispersed in water. The FSCPN was synthesized via the polycondensation of IPDI with multifunctional polyols and a diamine, which were selected for various reasons. For example, TFO was chosen to provide a low surface energy as the first required factor, and the applied content accounted for 3.60 wt % of the aqueous solution and represented 10.8 wt % of the resultant film. DMBA was employed to provide the water dispersibility, and PTMG was introduced as a flexible hydrophobic macrodiol. TMP was selected as a cross-linking agent to form branching bonds and thus undergo internal chemical (covalent) cross-linking. Meanwhile, a noncovalent physical cross-linking phenomenon was achieved via the macrocyclic urea hydrogen bonding that resulted from the reactions between EDA and IPDI. The chemical and physical synergistic cross-linking phenomena satisfied the second requirement outlined earlier. The average molecular weight between cross-links (M_c) could be calculated by dividing the total amount of materials by the molar number of cross-links,

DOI: 10.1021/acsami.9b01971
ACS Appl. Mater. Interfaces 2019, 11, 16914−16921

and the chemical and urea physical cross-linking densities ($\nu = 1/2M_c$) thus determined for FSCPN were 7.66×10^{-5} and 3.83×10^{-4} mol/g, respectively.[38] Furthermore, we envisioned that the FSCPN composite with suitable compatibility could form a homogeneous and amorphous material with a smooth surface, thus meeting the third and fourth required factors.

As we had anticipated, the SEM and EDX elemental mapping revealed that a smooth surface was obtained, and the fluorinated moieties were distributed uniformly both on the surface and throughout the matrix of the FSCPN film (Figure 1); thus, the first, third, and fourth required factors (low surface energy, homogeneous composition, and smoothness, respectively) were achieved. The EDX mappings of both sides of the film, and the surface elementary analysis via XPS provided in Figures S1 and S2 (Supporting Information) further demonstrated the homogeneous composition of the FSCPN film. The characterizations confirming the structure of FSCPN, including SEC analysis, TEM images, and FTIR spectra, are given in Figures S3−S5 (Supporting Information).

The TGA indicated that the film withstood temperatures of up to 200 °C without encountering mass loss (Figure S6, Supporting Information). The storage modulus (G'), loss modulus (G''), and tan δ (G''/G') curves obtained via DMA over the temperature range from −70 to 200 °C are given in Figure 2a. The glass transition temperature (T_g) as determined according to the tan δ (G''/G') curve was 58 °C, which was consistent with the value corresponding to the broad peak at ∼55 °C in the DSC curve (Figure S7, Supporting Information).[39] The film with this T_g will not undergo temperature-induced transitions if it is used at ambient temperatures, thus ensuring that the film will have suitable stability for various room-temperature applications.[40] Furthermore, the DSC curve did not exhibit any sharp peaks corresponding to crystallization over the range from −70 to 200 °C, confirming the amorphous nature of the FSCPN composite and thus fulfilling the third required factor.

Film samples with a thickness of 0.5 ± 0.1 mm exhibited an optical transmission exceeding 98% at 500 nm as seen in Figure 2b. The inset AFM image indicates that the roughness of the film surface was only in the range of several nanometers, which was close to the physical roughness limits and further demonstrated that a smooth surface was achieved.[41,42] The film was subsequently applied onto the screen of a mobile phone to demonstrate its possible application for electronic displays. As shown in the top region of the screen enclosed by the red dashed lines in Figure 2c, this transparent film did not obscure the screen. Moreover, the portion of the screen that was covered by the film retained its responsiveness to finger touch commands, further indicating its potential applicability for mobile electronic displays or devices (Movie S1, Supporting Information).

The FSCPN film exhibited free adhesion after it had been exposed to test liquids with various surface tensions including water, diiodomethane, and hexadecane (72.8, 50.8, and 27.5 mN/m, respectively, at 20 °C),[43] and oils with different viscosities such as cooking oil and pump oil (∼80 and 200 cP, respectively, at 20 °C). All of these liquids cleanly glided down the surface of the film without leaving any residue along their paths (Figure 2d and Movie S2, Supporting Information). Notably, these liquids were still able to slide off our film after an hour of contact. In addition, after the immersion of films in these liquids, the stained water (blue) did not wet the film, and all the other liquids had contracted and gradually flowed off this surface (Movie S3, Supporting Information). The CA, SA, θ_A, and θ_R of these test liquids are given in Table 1, with a liquid droplet volume of 2 μL employed for the CA tests and a 20 μL volume used for the SA tests. The CAs recorded at various times after the application of these liquids onto the film are provided in Figure S8 (Supporting Information). A minimum bending radius of less than 1 mm was reached, thus demonstrating that the film had a high degree of flexibility and foldability (Figure 2e).[44] The flexibility of the film was further illustrated by folding it into a crane shape without inducing damage (Figure 2f).

Table 1. CA, SA, θ_A, and θ_R of the Film toward Various Test Liquids

	water (deg)	diiodomethane (deg)	hexadecane (deg)	cooking oil (deg)	pump oil (deg)
CA	92 ± 2	65 ± 2	33 ± 2	57 ± 2	56 ± 3
SA	49 ± 1	12 ± 1	13 ± 1	18 ± 1	18 ± 1
θ_A	96 ± 2	69 ± 2	41 ± 1	64 ± 2	32 ± 2
θ_R	75 ± 3	52 ± 1	28 ± 2	35 ± 2	43 ± 2

Strikingly, a maximal fracture strain of up to 3100 ± 150% was achieved for a FSCPN film sample with a thickness, gauge length, and width of 0.5, 5, and 10 mm, respectively, at the stretching rates of 2−15 mm/min (Figure 3a and Movie S4, Supporting Information). In addition, the samples retained their transparency when they were elongated by 1900 ± 100%. Considering the maximum elongation of only 100−1100% that is achieved with typical silicon rubbers, it is apparent that the synergistic cross-linking in this work provided an impressive degree of stretchability.[45]

The film stretchability at various stretching rates is provided in Figure 3b, and the increased fracture tolerance observed as the stretching rate was decreased, which could be attributed to the greater amount of time available for the reformation of the cleaved physical bonds.[46] It was noteworthy that the tensile strength reached up to 44 MPa, and this excellent mechanical performance surpassed those achieved in many previously reported examples.[47] The excellent strength and toughness of the film was further demonstrated when it was employed to lift a 10 kg barbell (Figure 3c). To the best of our knowledge, only a few elastomers with much less tensile strength (<0.4 MPa) have exhibited higher stretchabilities, such as those based on metal−ligand complexes[48] or nanocomposite hydrogels.[49]

When the stretched film was released, the initial recovery proceeded rapidly and the transparency also exhibited self-healing behavior (Figure 3d and Movie S5, Supporting Information). The recovery ratios exhibited by the film that had been subjected to strain values of both 3000 and 1800% exceeded 80% after 5 min of recovery, over 90% after 30 min of recovery, and reached 95% after 24 h of recovery, as indicated by the free recovery processes of the films in Figure 3e. The stress−strain curves for each of the 10 stretch-and-recover cycles with elongations of 1800, 1000, 500, and 200%, respectively, demonstrated the sustained reversible stretchability of the film, although the tensile strength diminished as the number of cycles increased (Figure S9, Supporting Information).

More strikingly, all of the test liquids were found to cleanly slide off the stretched films, and the films retained their antiadhesion properties when they were elongated by up to 1800% (Figure 4a and Movie S6, Supporting Information).

DOI: 10.1021/acsami.9b01971
ACS Appl. Mater. Interfaces 2019, 11, 16914−16921

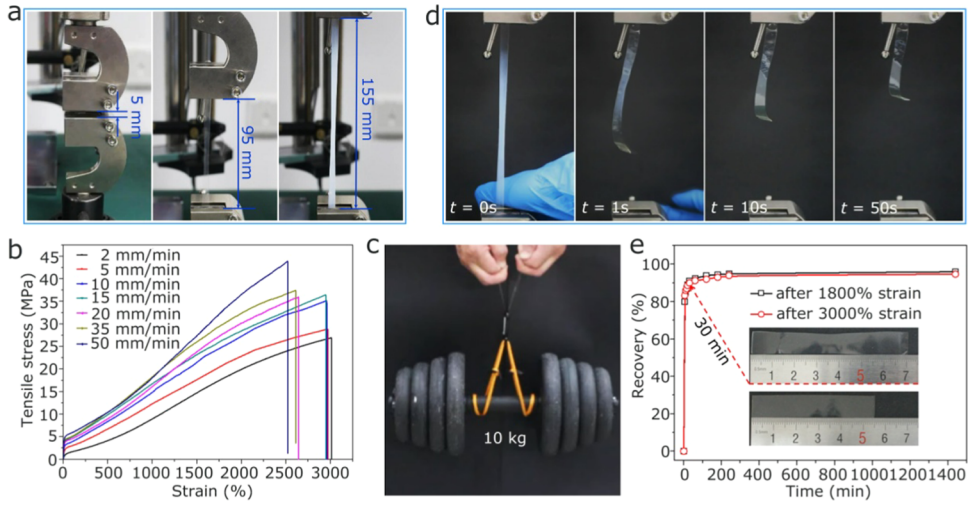

Figure 3. Stretchability, robustness, and recovery of the films. (a) Photographs of the film before and after stretching by up to 3000% at the stretching rate of 15 mm/min. Transparency was retained after stretching by up to 1800%. (b) The stress−strain curves of the films stretched at various rates. (c) Photograph demonstrating the excellent strength and toughness of the film. (d) The rapid initial recovery of the film after it had been stretched by 3000% at 15 mm/min and subsequently released. (e) The recovery of the film after it had been stretched by 3000 and 1800% at 15 mm/min. The inset photographs show the recovered film after its elongation by 3000% and the original film prior to stretching.

The CAs and SAs of these liquids on the films that had been stretched to different degrees are provided in Figure 4b,c. Although all of the test liquids could slide cleanly off these films, the contact angles became smaller, whereas the sliding angles grew larger when the film was subjected to greater elongation. When the films were stretched by more than 1800%, the liquids slid off the surfaces but left residue along their pathways.

As the loss of both antiadhesion properties and transparency was observed when the film elongation exceeded 1800%, we suspect that the film may have undergone a strain-induced structural change, which likely disrupted the four previously mentioned factors and thus degraded these properties. This consideration inspired us to investigate the structural changes that may have occurred during stretching, whereas the extreme tensile strength and strain performance as well as the rapid reversibility impeded most of these characterizations. Optical microscopy images of the film with 2500% strain (Figure 4d) and those obtained under various stretching states during a full stretching and 24 h recovery process are shown in Figure 4e. When the deformation exceeded 1800%, a lamellar structure that was aligned in an orthogonal direction toward the stretching direction was observed, and the amorphous nature as well as the smoothness were lost, so that the third and fourth required factors were thus unsatisfied. Although seldom directly observed, this structure was commonly considered as a local ordered structure that arose due to stretching-induced polymer chain alignment and packing, and structures formed in the perpendicular direction were attributed to the mechanical torque required to prevent excessive local stress.[50,51] During the recovery process, the ordered structure disappeared in a reversible manner, thus facilitating the recovery of the antiadhesion properties and transparency. This reversible behavior also provides the film with potential applications as a self-healing and strain-responsive smart material.

To better demonstrate the synergistic effect of cross-linking as the second required factor, we compared the properties of the FSCPN film with those of two other films, including a fluorine-terminated polyurethane network with physical-cross-linking (FPN-P) film that lacked chemical cross-linking and another fluorine-terminated polyurethane network with chemical-cross-linking (FPN-C) film that lacked urea-based physical cross-linking. With regard to the structural designs, the TMP units were replaced by ethanediol with an equal quantity of hydroxyl groups for the preparation of FPN-P to thus eliminate the branching bonds. Meanwhile, an equimolar quantity of ethanediol was used instead of EDA during the preparation of FPN-C to remove the urea-based hydrogen bonds.

Notably, in the absence of the cooperatively enhanced effects of the chemical and physical cross-linking, test liquids were found to adhere to both the FPN-P and FPN-C films (Figure S10, Supporting Information). Furthermore, the maximum stretchabilities of the FPN-P and FPN-C films were both significantly decreased to 1050 ± 100% strain, and the tensile strengths were also dramatically reduced to 12 and 5 MPa, respectively, as indicated by the stress−strain images and curves of the films (Figure 4f,g). The recovery capabilities of these films had also significantly diminished (Figures 4h and S11, Supporting Information). After they were elongated by 1000%, the FPN-P and FPN-C films, respectively, exhibited recovery ratios of 68 and 55% after 5 min of recovery, 77 and 64% after 30 min of recovery, and 88 and 75% after 24 h of recovery.

The chemical and physical cross-linking phenomena combined as the second required factor were thus found to enhance both the antiadhesion properties and the stretchability of the film. Although chemical cross-linking has been used previously to enhance liquid repellency, the effect of physical cross-linking was for the first time presented and experimentally confirmed in this work.[52,53]

Interestingly, only the FPN-P film exhibited a reversible strain-induced opaqueness and microscopic lamellar structure, which was similar to that of the FSCPN film. This demonstrated the crucial effect of urea-based hydrogen bonds in enabling the exchange of hydrogen-bonded pairs when the polymer chains became interpenetrated during the polymer chain alignment and packing process (Figure S12,

DOI: 10.1021/acsami.9b01971
ACS Appl. Mater. Interfaces 2019, 11, 16914−16921

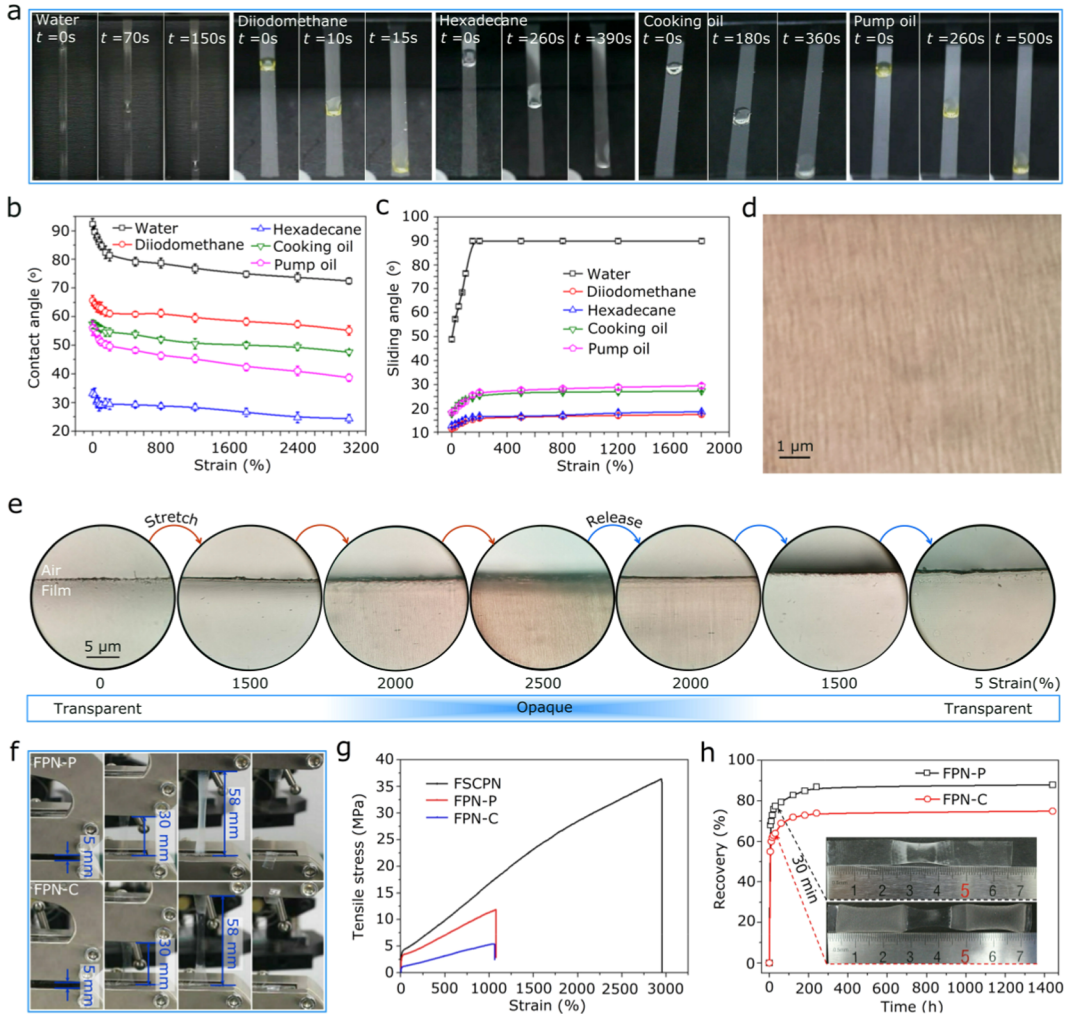

Figure 4. Antiadhesion performance and transparency of the films under significant deformations. (a) The test liquids cleanly slid off films that were stretched by 1800%. CA (b) and SA (c) on the FSCPN films with different strains. (d) The enlarged morphologies of the film that had been elongated by 2500%. (e) Optical microscopy images depicting the morphologies of the film at different elongation degrees recorded during an entire stretching and 24 h recovery cycle. (f) Photographs of the FPN-P and FPN-C films when they were stretched at 15 mm/min and fractured. (g) The stress–strain curves of the FSCPN, FPN-P, and FPN-C at 15 mm/min. (h) The 24 h recovery of the FPN-P and FPN-C films after they have been stretched by 1000% at 15 mm/min.

Supporting Information). In addition to the slower recovery in comparison with the FSCPN film, the time-dependence of the structural development for the FPN-P film was also observed during the recovery process. The disappearance of these lamellar structures as well as the self-healing of transparency required extra time (~6 h) after the release of the film from a 1000% strain to a smaller 500% strain.

4. CONCLUSIONS

In summary, the present work demonstrates that four essential criteria including the use of a low-surface-energy component, a chemical and physical synergistic cross-linking, a homogeneous and amorphous composite, and a smooth material surface can be successfully employed to achieve a FSCPN polymer film exhibiting antiadhesion performance and transparency even under significant deformations. The combination of desirable properties such as the adhesion-resistance to various liquids under large deformations, reversible elongation by up to 3000% with a tensile strength of over 44 MPa, optical transmission in excess of 98% at a thickness of 0.5 mm, and its facile and scalable preparation ensure that this material will have a wide range of potential applications.

■ ASSOCIATED CONTENT

Ⓢ Supporting Information

The Supporting Information is available free of charge on the ACS Publications website at DOI: 10.1021/acsami.9b01971.

EDX mapping of the top and opposite surfaces of the FSCPN film; XPS analysis of the top and opposite surfaces of the FSCPN film; SEC trace of FSCPN; TEM image of FSCPN aqueous solution; FTIR spectrum of the FSCPN film; TGA thermograms of the FSCPN film; DSC thermograms of the FSCPN film; contact angles of water, diiodomethane, hexadecane, cooking oil, and pump oil recorded at various times after their application onto the FSCPN film; stress–strain curves of the films stretched at 15 mm/min for each of the 10 stretching and recovery cycles with the elongation of 1800, 1000, 500, and 200%, respectively; various liquids strongly adhere to the FPN-P and FPN-C films; time-lapsed recovery of the FPN-P and FPN-C films after 1000%

DOI: 10.1021/acsami.9b01971
ACS Appl. Mater. Interfaces 2019, 11, 16914–16921

strain; microphotograph of the FPN-P and FPN-C films with different strains (PDF)

Portion of the screen covered by the film retained its responsiveness to finger touch commands (AVI)

Liquids gliding down the surface of the film (AVI)

Immersion of films in liquids (AVI)

Maximal fracture strain for FSCPN film sample (AVI)

Release of stretched film (AVI)

Sliding-off of test liquids (AVI)

AUTHOR INFORMATION

Corresponding Author

*E-mail: xuwu@gzhu.edu.cn.

ORCID

Hui Yang: 0000-0001-6750-4551

Jinben Wang: 0000-0002-6360-9572

Xu Wu: 0000-0002-8907-6073

Author Contributions

X.W. conceived the experiments and wrote the manuscript. M.L., F.L., X.X., and D.Y. participated in the materials preparation and characterization. H.Y. and J.W. performed the AFM and XPS measurements. All authors were involved in analyzing the results and revising the manuscript.

Notes

The authors declare no competing financial interest.

ACKNOWLEDGMENTS

We gratefully thank the Important National Science and Technology Specific Project of China (2017ZX05013003004), the National Natural Science Foundations of China (21878059 and 21603240), the Science and Technology Project of Guangdong Province (2017A050501040), and the Science and Technology Project of Guangzhou City (201610010018) for sponsoring this research.

REFERENCES

(1) Chu, B.; Burnett, W.; Chung, J. W.; Bao, Z. N. Bring on the BodyNET. *Nature* **2017**, *549*, 328−330.

(2) Larson, C.; Peele, B.; Li, S.; Robinson, S.; Totaro, M.; Beccai, L.; Mazzolai, B.; Shepherd, R. Highly Stretchable Electroluminescent Skin for Optical Signaling and Tactile Sensing. *Science* **2016**, *351*, 1071−1074.

(3) Aliev, A. E.; Oh, J.; Kozlov, M. E.; Kuznetsov, A. A.; Fang, S. L.; Fonseca, A. F.; Ovalle, R.; Lima, M. D.; Haque, M. H.; Gartstein, Y. N.; Zhang, M.; Zakhidov, A. A.; Baughman, R. H. Giant-Stroke, Superelastic Carbon Nanotube Aerogel Muscles. *Science* **2009**, *323*, 1575−1578.

(4) Baughman, R. H. Materials Science. Playing Nature's Game with Artificial Muscles. *Science* **2005**, *308*, 63−65.

(5) Kim, C. C.; Lee, H. H.; Oh, K. H.; Sun, J. Y. Highly Stretchable, Transparent Ionic Touch Panel. *Science* **2016**, *353*, 682−687.

(6) Sekitani, T.; Nakajima, H.; Maeda, H.; Fukushima, T.; Aida, T.; Hata, K.; Someya, T. Stretchable Active-Matrix Organic Light-Emitting Diode Display Using Printable Elastic Conductors. *Nat. Mater.* **2009**, *8*, 494−499.

(7) Liu, Z. F.; Fang, S.; Moura, F. A.; Ding, J. N.; Jiang, N.; Di, J.; Zhang, M.; Lepró, X.; Galvão, D. S.; Haines, C. S.; Yuan, N. Y.; Yin, S. G.; Lee, D. W.; Wang, R.; Wang, H. Y.; Lv, W.; Dong, C.; Zhang, R. C.; Chen, M. J.; Yin, Q.; Chong, Y. T.; Zhang, R.; Wang, X.; Lima, M. D.; Ovalle-Robles, R.; Qian, D.; Lu, H.; Baughman, R. H. Hierarchically Buckled Sheath-Core Fibers for Superelastic Electronics, Sensors, and Muscles. *Science* **2015**, *349*, 400−404.

(8) Wang, X. D.; Dong, L.; Zhang, H. L.; Yu, R. M.; Pan, C. F.; Wang, Z. L. Recent Progress in Electronic Skin. *Adv. Sci.* **2015**, No. 1500169.

(9) Chortos, A.; Bao, Z. N. Skin-Inspired Electronic Devices. *Mater. Today* **2014**, *17*, 321−331.

(10) Chu, Z.; Seeger, S. Superamphiphobic Surfaces. *Chem. Soc. Rev.* **2014**, *43*, 2784−2798.

(11) Wong, T. S.; Sun, T.; Feng, L.; Aizenberg, J. Interfacial Materials with Special Wettability. *MRS Bull.* **2013**, *38*, 366−371.

(12) Kota, A. K.; Kwon, G.; Tuteja, A. The Design and Applications of Superomniphobic Surfaces. *NPG Asia Mater.* **2014**, *6*, No. e109.

(13) Tuteja, A.; Choi, W.; Ma, M.; Mabry, J. M.; Mazzella, S. A.; Rutledge, G. C.; McKinley, G. H.; Cohen, R. E. Designing Superoleophobic Surfaces. *Science* **2007**, *318*, 1618−1622.

(14) Barthlott, W.; Neinhuis, C. Purity of the Sacred Lotus, or Escape from Contamination in Biological Surfaces. *Planta* **1997**, *202*, 1−8.

(15) Wang, S. L.; Zhang, W. W.; Yu, X. Q.; Liang, C. H.; Zhang, Y. F. Sprayable Superhydrophobic Nano-Chains Coating with Continuous Self-Jumping of Dew and Melting Frost. *Sci. Rep.* **2017**, *7*, No. 40300.

(16) Wong, T. S.; Kang, S. H.; Tang, S. K. Y.; Smythe, E. J.; Hatton, B. D.; Grinthal, A.; Aizenberg, J. Bioinspired Self-Repairing Slippery Surfaces with Pressure-Stable Omniphobicity. *Nature* **2011**, *477*, 443−447.

(17) Amini, S.; Kolle, S.; Petrone, L.; Ahanotu, O.; Sunny, S.; Sutanto, C. N.; Hoon, S.; Cohen, L.; Weaver, J. C.; Aizenberg, J.; Vogel, N.; Miserez, A. Preventing Mussel Adhesion Using Lubricant-Infused Materials. *Science* **2017**, *357*, 668−673.

(18) Cui, J. X.; Daniel, D.; Grinthal, A.; Lin, K. X.; Aizenberg, J. Dynamic Polymer Systems with Self-Regulated Secretion for the Control of Surface Properties and Material Healing. *Nat. Mater.* **2015**, *14*, 790−795.

(19) Garrett, A. B. Teflon: Roy J. Plunkett. *J. Chem. Educ.* **1962**, *39*, 288.

(20) Makinson, K. R.; Tabor, D. Friction and Transfer of Polytetrafluoroethylene. *Nature* **1964**, *201*, 464−466.

(21) Kaelble, D. H.; Uy, K. C. A Reinterpretation of Organic Liquid-Polytetrafluoroethylene Surface Interactions. *J. Adhes.* **1970**, *2*, 50−60.

(22) Hu, X.; Tang, C. Y.; He, Z. K.; Shao, H.; Xu, K. Q.; Mei, J.; Lau, W. M. Water-Proof Protection: Highly Stretchable Superhydrophobic Composite Coating Based on Self-Adaptive Deformation of Hierarchical Structures. *Small* **2017**, *13*, No. 1602353.

(23) Wang, S. L.; Yu, X. Q.; Zhang, Y. F. Large-Scale Fabrication of Translucent, Stretchable and Durable Superhydrophobic Composite Films. *J. Mater. Chem. A* **2017**, *5*, 23489−23496.

(24) Davis, A.; Surdo, S.; Caputo, G.; Bayer, I. S.; Athanassiou, A. Environmentally Benign Production of Stretchable and Robust Superhydrophobic Silicone Monoliths. *ACS Appl. Mater. Interfaces* **2018**, *10*, 2907−2917.

(25) Yao, X.; Hu, Y. H.; Grinthal, A.; Wong, T. S.; Mahadevan, L.; Aizenberg, J. Adaptive Fluid-Infused Porous Films with Tunable Transparency and Wettability. *Nat. Mater.* **2013**, *12*, 529−534.

(26) Cheng, D. F.; Urata, C.; Yagihashi, M.; Hozumi, A. A Statically Oleophilic but Dynamically Oleophobic Smooth Nonperfluorinated Surface. *Angew. Chem., Int. Ed.* **2012**, *51*, 2956−2959.

(27) Wang, L.; McCarthy, T. J. Covalently Attached Liquids: Instant Omniphobic Surfaces with Unprecedented Repellency. *Angew. Chem., Int. Ed.* **2016**, *128*, 252−256.

(28) Rabnawaz, M.; Liu, G. J. Graft-Copolymer-Based Approach to Clear, Durable, and Anti-Smudge Polyurethane Coatings. *Angew. Chem., Int. Ed.* **2015**, *54*, 6516−6520.

(29) Hu, H.; Wang, J.; Wang, Y.; Gee, E.; Liu, G. J. Silicone-Infused Antismudge Nanocoatings. *ACS Appl. Mater. Interfaces* **2017**, *9*, 9029−9037.

(30) Zheng, C.; Liu, G. J.; Hu, H. UV-Curable Antismudge Coatings. *ACS Appl. Mater. Interfaces* **2017**, *9*, 25623−25630.

(31) Wu, X.; Zhang, Y. C.; Liu, M. H.; Xu, X. B.; Wang, Z. P.; Wyman, I.; Yang, H.; Liu, F. H.; Wang, J. B.; Wu, J. Z. Preventing

DOI: 10.1021/acsami.9b01971
ACS Appl. Mater. Interfaces 2019, 11, 16914−16921

Crude Oil Adhesion using Fully Waterborne Coatings. *AIChE J.* **2019**, No. e16569.
(32) Uehara, H.; Yamanobe, T.; Yukawa, Y.; Matsuoka, Y. Method of Manufacture of Polytetrafluoroethylene Stretched Film, and Polytetrafluoroethylene Stretched Film. U.S. Patent USPCT/US90/01236, 1990.
(33) Duperray, G.; Monnet, A.; Tournut, C. Method of Molding Polytetrafluoroethylene. U.S. Patent US671042, 1978.
(34) Bodö, P.; Schott, M. Highly Oriented Polytetrafluoroethylene Films: A Force Microscopy Study. *Thin Solid Films* **1996**, *286*, 98−106.
(35) Liu, M. J.; Wang, S. T.; Jiang, L. Nature-Inspired Superwettability Systems. *Nat. Rev. Mater.* **2017**, *2*, No. 17036.
(36) Yong, J. L.; Chen, F.; Yang, Q.; Huo, J. L.; Hou, X. Superoleophobic Surfaces. *Chem. Soc. Rev.* **2017**, *46*, 4168−4217.
(37) Li, Q. H.; Lee, B. J.; Zhang, Z. M.; Allen, D. W. Light Scattering of Semitransparent Sintered Polytetrafluoroethylene Films. *J. Biomed. Opt.* **2008**, *13*, No. 054064.
(38) Valentín, J. L.; Carretero-González, J.; Mora-Barrantes, I.; Chassé, W.; Saalwächter, K. Uncertainties in the Determination of Cross-Link Density by Equilibrium Swelling Experiments in Natural Rubber. *Macromolecules* **2008**, *41*, 4717−4729.
(39) Yanagisawa, Y.; Nan, Y. L.; Okuro, K.; Aida, T. Mechanically Robust, Readily Repairable Polymers via Tailored Noncovalent Cross-Linking. *Science* **2018**, *359*, 72−76.
(40) Xiao, X. L.; Kong, D. Y.; Qiu, X. Y.; Zhang, W. B.; Zhang, F. H.; Liu, L. W.; Liu, Y. J.; Zhang, S.; Hu, Y.; Leng, J. S. Shape-Memory Polymers with Adjustable High Glass Transition Temperatures. *Macromolecules* **2015**, *48*, 3582−3589.
(41) Xu, Q. B.; Mayers, B. T.; Lahav, M.; Vezenov, D. V.; Whitesides, G. M. Approaching Zero: Using Fractured Crystals in Metrology for Replica Molding. *J. Am. Chem. Soc.* **2005**, *127*, 854−855.
(42) Matsunaga, M.; Aizenberg, M.; Aizenberg, J. Controlling the Stability and Reversibility of Micropillar Assembly by Surface Chemistry. *J. Am. Chem. Soc.* **2011**, *133*, 5545−5553.
(43) Hu, H.; Liu, G. J.; Wang, J. Clear and Durable Epoxy Coatings that Exhibit Dynamic Omniphobicity. *Adv. Mater. Interfaces* **2016**, *3*, No. 1600001.
(44) Liang, L. R.; Gao, C. Y.; Chen, G. M.; Guo, C. Y. Large-Area, Stretchable, Super Flexible and Mechanically-Stable Thermoelectric Films of Polymer/Carbon Nanotube Composites. *J. Mater. Chem. C* **2016**, *4*, 526−532.
(45) Bhowmick, A. K.; Stephens, H. *Handbook of Elastomers*, 2nd ed.; CRC Press: Boca Raton, 2000.
(46) Li, C. H.; Wang, C.; Keplinger, C.; Zuo, J. L.; Jin, L. H.; Sun, Y.; Zheng, P.; Cao, Y.; Lissel, F.; Linder, C.; You, X. Z.; Bao, Z. N. A Highly Stretchable Autonomous Self-Healing Elastomer. *Nat. Chem.* **2016**, *8*, 618−624.
(47) Fang, F.; Li, Y. Q.; Xiao, H. M.; Hu, N.; Fu, S. Y. Layer-Structured Silver Nanowire/Polyaniline Composite Film as High Performance X-Band EMI Shielding Material. *J. Mater. Chem. C* **2016**, *4*, 4193−4203.
(48) Rao, Y. L.; Chortos, A.; Pfattner, R.; Lissel, F.; Chiu, Y. C.; Feig, V.; Xu, J.; Kurosawa, T.; Gu, X. D.; Wang, C.; He, M. Q.; Chung, J. W.; Bao, Z. N. Stretchable Self-Healing Polymeric Dielectrics Cross-Linked Through Metal-Ligand Coordination. *J. Am Chem. Soc.* **2016**, *138*, 6020−6027.
(49) Liu, R. Q.; Liang, S. M.; Tang, X. Z.; Yan, D.; Li, X. F.; Yu, Z. Z. Tough and Highly Stretchable Grapheme Oxide/Polyacrylamide Nanocomposite Hydrogels. *J. Mater. Chem.* **2012**, *22*, 14160−14167.
(50) Higaki, Y. J.; Suzuki, K.; Ohta, N.; Takahara, A. Strain-Induced Molecular Aggregation States Around a Crack Tip in a Segmented Polyurethane Film under Uniaxial Stretching. *Polymer* **2017**, *116*, 458−465.
(51) Yeh, F. J.; Hsiao, B. S.; Sauer, B. B.; Michel, S.; Siesler, H. W. In-Situ Studies of Structure Development During Deformation of a Segmented Poly(urethane-urea) Elastomer. *Macromolecules* **2003**, *36*, 1940−1954.
(52) Rabnawaz, M.; Liu, G. J.; Hu, H. Fluorine-Free Anti-Smudge Polyurethane Coatings. *Angew. Chem., Int. Ed.* **2015**, *54*, 12722−12727.
(53) Wu, X.; Liu, M. H.; Zhong, X. M.; Liu, G. J.; Wyman, I.; Wang, Z. P.; Wu, Y. Q.; Yang, H.; Wang, J. B. Smooth Water-Based Antismudge Coatings for Various Substrates. *ACS Sustainable Chem. Eng.* **2017**, *5*, 2605−2613.

DOI: 10.1021/acsami.9b01971
ACS Appl. Mater. Interfaces 2019, 11, 16914−16921